

Drift of scroll waves in thin layers caused by thickness features

I.V. Biktasheva,¹ H. Dierckx,² and V.N. Biktashev³

¹Department of Computer Science, University of Liverpool, Liverpool L69 3BX, UK

²Department of Mathematical Physics and Astronomy, Ghent University, 9000 Ghent, Belgium

³College of Engineering, Mathematics and Physical Sciences, University of Exeter, Exeter EX4 4QF, UK

(Dated: December 6, 2024)

A scroll wave in a very thin layer of excitable medium is similar to a spiral wave, but its behaviour is affected by the layer geometry. We identify the effect of sharp variations of the layer thickness, which is separate from filament tension and curvature-induced drifts described earlier. We sketch a two-step asymptotic theory describing this effect, including averaging through the layer thickness and then drift of perturbed spiral waves using response functions. As specific examples, we consider drift of scrolls along thickness steps, ridges, ditches, and disk-shape thickness variations. Asymptotic predictions agree with numerical simulations.

PACS numbers: 02.70.-c, 05.10.-a, 82.40.Bj, 82.40.Ck, 87.10.-e

Spiral waves in two dimensions (2D) and scroll wave in three dimensions (3D) are regimes of self-organization observed in physical, chemical and biological dissipative systems [1]. A particularly important example is re-entrant arrhythmias in the heart [2]. In nature, 2D systems are often thin layers of 3D media, and geometry of such layers affects the dynamics of spiral/scroll waves. Known phenomena include scroll filament tension [3] and layer curvature [4], which can cause spiral waves to drift to/from thinner regions and more curved regions of the 2D excitable sheet respectively. Here we consider effects caused by *sharp features* of the layer thickness. There is experimental evidence that such effects play significant role in atrial fibrillation [5, 6]. Here we analyse these effects theoretically by a combination of asymptotic and numerical methods, for two selected archetypical models. We start from a generic homogeneous isotropic reaction-diffusion system in 3D:

$$\mathbf{v}_t = \mathbf{f}(\mathbf{v}) + \mathbf{D}\nabla^2\mathbf{v}, \quad (1)$$

where $\mathbf{v} = \mathbf{v}(\vec{r}, t)$, $\vec{r} = (x, y, z)$. In numerical examples, we use excitable FitzHugh-Nagumo system, with kinetics

$$\mathbf{f} : \begin{bmatrix} u \\ v \end{bmatrix} \mapsto \begin{bmatrix} \alpha^{-1}(u - u^3/3 - v) \\ \alpha(u + \beta - \gamma v) \end{bmatrix} \quad (2)$$

for $\alpha = 0.3$, $\beta = 0.68$, $\gamma = 0.5$, and $\mathbf{D} = \text{diag}(1, 0)$, and self-oscillatory Oregonator model, with kinetics

$$\mathbf{f} : \begin{bmatrix} u \\ v \end{bmatrix} \mapsto \begin{bmatrix} p^{-1} \left(u(1-u) - fv \frac{u-q}{u+q} \right) \\ u - v \end{bmatrix} \quad (3)$$

for $p = 0.1$, $f = 1.5$, $q = 0.002$, and $\mathbf{D} = \text{diag}(1, 0.6)$ [7].

We consider system (1) in a thin layer, $z \in [z_{\min}(x, y), z_{\max}(x, y)]$, $(x, y) \in \mathbb{R}^2$, with no-flux boundaries at $z = z_{\min}$ and $z = z_{\max}$. Let $H(x, y) \equiv z_{\max}(x, y) - z_{\min}(x, y)$ be uniformly small, $0 < H(x, y) \leq \mu \ll 1$. Then we show by formal asymptotic methods [7] that

$$\mathbf{v}(x, y, z, t) = \mathbf{u}(x, y, t) + \mathcal{O}(\mu^2), \quad (4)$$

and Eq. (1) in the leading order in μ reduces to the following 2D approximation:

$$\mathbf{u}_t = \mathbf{f}(\mathbf{u}) + \mathbf{D} \frac{1}{H(x, y)} \nabla \cdot (H(x, y) \nabla \mathbf{u}) + \mathcal{O}(\mu^2) \quad (5)$$

We rewrite Eq. (5) in the form

$$\mathbf{u}_t = \mathbf{f}(\mathbf{u}) + \mathbf{D}\nabla^2\mathbf{u} + \epsilon\mathbf{h}(\mathbf{u}, x, y, \nabla) \quad (6)$$

where

$$\epsilon\mathbf{h} = \epsilon\mathbf{D}(\nabla K) \cdot (\nabla \mathbf{u}), \quad \epsilon K = \ln H. \quad (7)$$

We treat (6,7) as a perturbation problem with the formal small parameter ϵ (which is distinct from the small parameter μ). We assume existence of a rigidly rotating spiral wave solution \mathbf{U} at $\epsilon = 0$.

For $K = K(x)$, we have $\epsilon\mathbf{h} = \epsilon\mathbf{D}K_x\mathbf{u}_x$. Let us consider first a step in thickness, i.e.

$$H(x, y) = \begin{cases} H_+, & x > x_s, \\ H_-, & x < x_s. \end{cases} \quad (8)$$

Then we have $\epsilon K = \ln(H_-) + \epsilon\Theta(x - x_s)$, $\epsilon = \ln(H_+/H_-)$, and

$$\epsilon\mathbf{h} = \epsilon\delta(x - x_s)\mathbf{D}\mathbf{u}_x. \quad (9)$$

Eqs. (12,13,14) of [8] predict the drift velocity via

$$\epsilon^{-1} \frac{d\vec{R}}{dt} = \vec{F}(\vec{R}) = (F_x, F_y), \quad (10)$$

$$F(\vec{R}) = F_x + iF_y = \int_0^\infty \oint \mathbf{W}(r, \theta)^+ \boldsymbol{\alpha}(r, \theta; \vec{R}) d\theta r dr, \quad (11)$$

$$\boldsymbol{\alpha}(r, \theta; \vec{R}) = \oint e^{-i\phi} \tilde{\mathbf{h}}(\mathbf{U}, r, \theta, \phi) \frac{d\phi}{2\pi}, \quad (12)$$

where $\tilde{\mathbf{h}}$ is the perturbation \mathbf{h} , calculated for $\mathbf{u} = \mathbf{U}$ and considered in the frame corotating with the spiral, and \mathbf{W} are

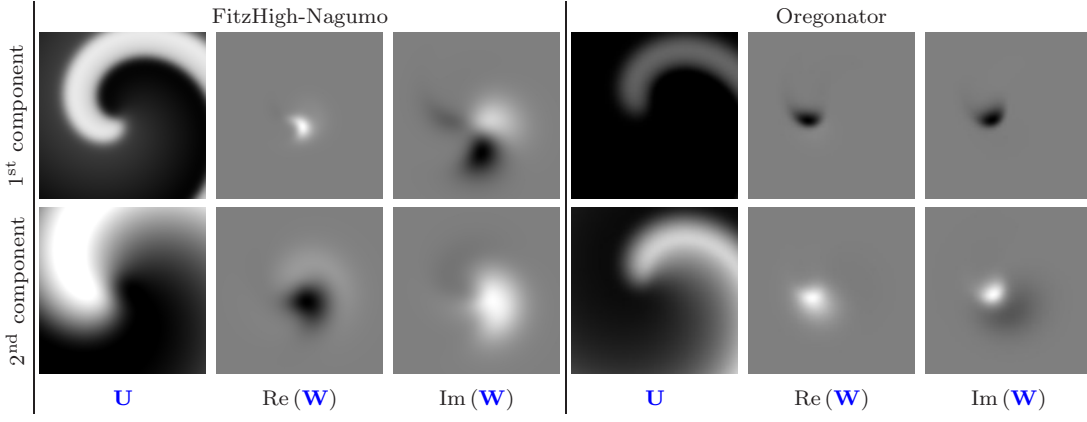


FIG. 1. Density plots of the spiral waves \mathbf{U} and response functions \mathbf{W} of the FitzHugh-Nagumo system (2) (central fragment 12.5×12.5) and Oregonator model (3) (central fragment 15×15). Grey periphery of \mathbf{W} components corresponds to zero, i.e. \mathbf{W} are well localized ensuring convergence of integrals (11).

(spatial) response functions of the spirals. The spirals and their response functions calculated for the two selected models using `DXSpiral` [7, 9] are illustrated in fig. 1. Evaluation of integral (12) with account of (9) and the coordinate transformations $\mathbf{h}(\vec{R}, t) = \hat{\mathbf{h}}(r, \theta, \phi)$, $\vec{R} = (X, Y)$, $\vec{r} = (x, y)$, $d = X - x_s$, $\theta = \vartheta(\vec{r} - \vec{R}) + \phi$, $r = \rho(\vec{r} - \vec{R})$, $x + iy \equiv \rho(\vec{r}) \exp(i\vartheta(\vec{r}))$ gives

$$\alpha = \begin{cases} 0, & r \leq |d|, \\ \frac{\mathbf{D}e^{-i\theta}}{\pi\sqrt{r^2 - d^2}} \left[\frac{d^2}{r^2} \mathbf{U}_r - \frac{i(r^2 - d^2)}{r^3} \mathbf{U}_\theta \right], & r > |d|. \end{cases} \quad (13)$$

Eqs. (11) and (13) define the specific force produced by the thickness step which depends only on the distance between the current spiral centre and the step line and is an even function about the position of the step,

$$F(\vec{R}) = S(d), \quad d \equiv X - x_s, \quad (14)$$

$$S(-d) = S(d) = S_x(d) + iS_y(d). \quad (15)$$

The components of the function $S(d)$ for the two selected models are shown in fig. 2(b,e). The important feature are zeros of S_x for $d = \pm d^*$ in both models. Assuming without loss of generality $x_s = 0$, the drift of a spiral is then described asymptotically by

$$\frac{dX}{dt} = \epsilon S_x(X), \quad \frac{dY}{dt} = \epsilon S_y(X), \quad \epsilon = \ln \left(\frac{H_+}{H_-} \right). \quad (16)$$

Fig. 2 illustrates predictions of the theory for the case of the stepwise thickness inhomogeneity and its comparison with the direct numerical simulations of both the 2D thickness-reduced system (5) and the full 3D system (1). Numerical simulations for both selected models were done with `BeatBox` [7, 10]. The relevant attractor for (16) is

$$X = -d^*, \quad Y = Y_0 + \epsilon S_y(-d^*)t, \quad (17)$$

where $S_x(-d^*) = 0$, $S_x'(-d^*) < 0$. That is, in both models the spiral attaches to the step at its thinner side and drifts along with the speed $|S_y(-d)|/0$. The speed of the drift is proportional to $\epsilon = \ln(H_+/H_-)$, and the direction of the drift depends on the spiral chirality: compare panels (a) and (d).

Now let us consider the following thickness profile: for some $x_\ell < x_r$,

$$H(x, y) = \begin{cases} H_o, & x < x_\ell, \\ H_i, & x_\ell < x < x_r, \\ H_o, & x_r < x, \end{cases} \quad (18)$$

which means a ‘‘ridge’’ for $H_i > H_o$ and a ‘‘ditch’’ for $H_i < H_o$. This case is easily reduced to the previous because

$$H(x, y) = H_i + (H_o - H_i) (\Theta(x - x_\ell) - \Theta(x - x_r)),$$

hence the formal perturbation is

$$\epsilon \mathbf{h} = \epsilon [\delta(x - x_\ell) - \delta(x - x_r)] \mathbf{D}u_x$$

where $\epsilon = \ln(H_i/H_o)$. Let $x_\ell = x_s - w/2$, $x_r = x_s + w/2$. We use the linearity of (10)–(12) and the previous result to get the interaction force in the form

$$F(\vec{R}) = T(d; w) = -T(-d; w), \quad d \equiv X - x_s,$$

$$T = T_x + iT_y = S \left(d + \frac{w}{2} \right) - S \left(d - \frac{w}{2} \right).$$

Fig. 3(a,b) shows the components of $T(d; w)$ for two selected values of the ridge width w , illustrating a pitchfork bifurcation of T_x roots. The bifurcation condition $T_x(d; w) = \partial_d T_x(d; w) = 0$, observation that the bifurcation happens at $d^* = 0$ and evenness of $S(d)$ gives the critical value of width implicitly via $S_x'(w^*/2) = 0$. For the FHN system, there are two positive roots for $S_x'(\cdot)$ (see fig. 2(b)), the smaller giving $w^* \approx 1.769$. Fig. 3(c,d) illustrates the drift along a cuneiform ditch, which may be in the first approximation considered a negative ditch with almost constant but slowly varying width. The bifurcation width w^* is designated by the dashed horizontal line. We see that below this line the spiral wave drifts in accordance with the theory prediction but slows down markedly in the vicinity of this line. It does not stop completely but proceeds further, albeit at a much slower speed. This is due to the ‘‘wedging’’ effect of the varying width: at $w \geq w^*$, the forces from the two opposite steps making the banks of the ditch, do not compensate each other exactly due to the angle between them. To estimate roughly

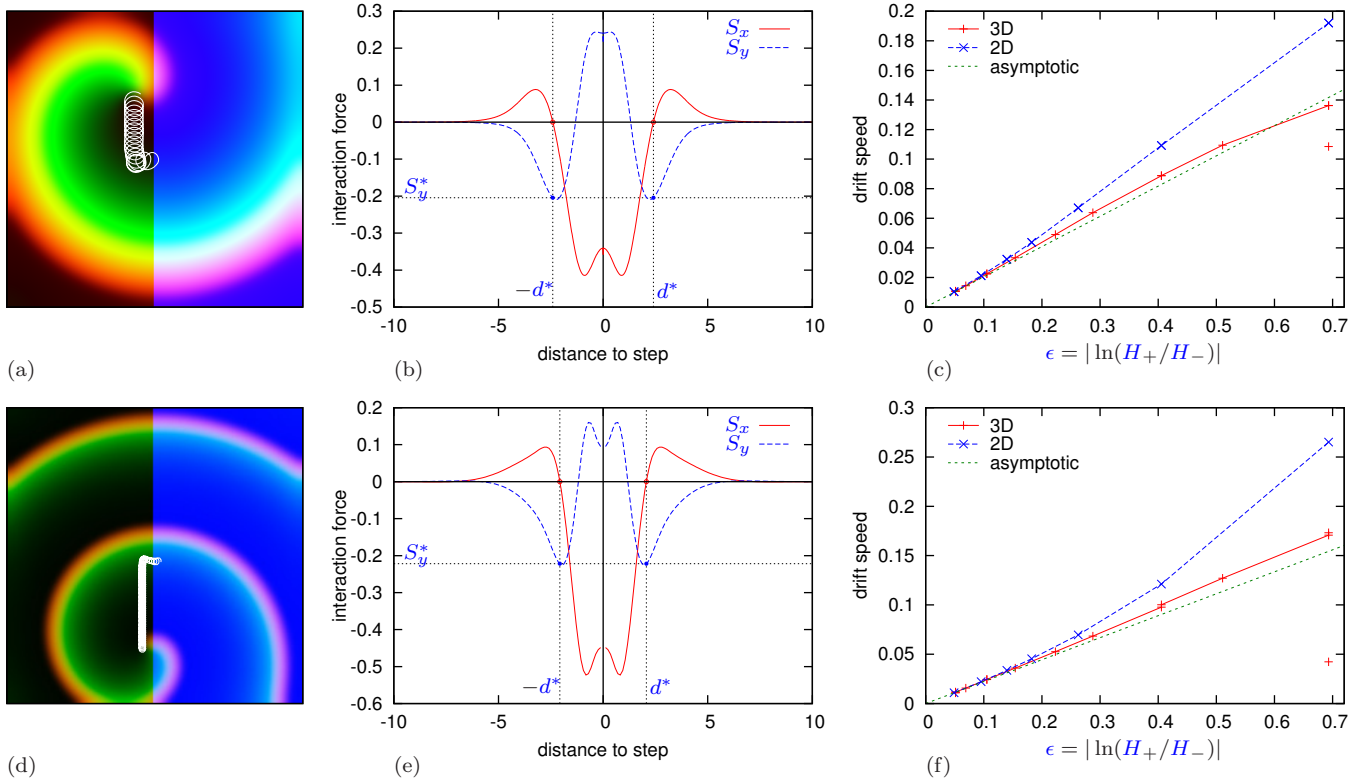


FIG. 2. Results of asymptotic theory of interaction with thickness step, and comparison with DNS. (a)–(c): FitzHugh-Nagumo system (2). (d)–(f): Oregonator model (3). (a),(d): Spiral wave snapshot (red color component: u field, green color component: v field, blue color component: H field), with the previous tip trajectory (white line). (b),(e): Components of the step interaction function (15). (c),(f): Drift of speed along the step in 3D system (1), 2D system (5) and asymptotic predicted by (17).

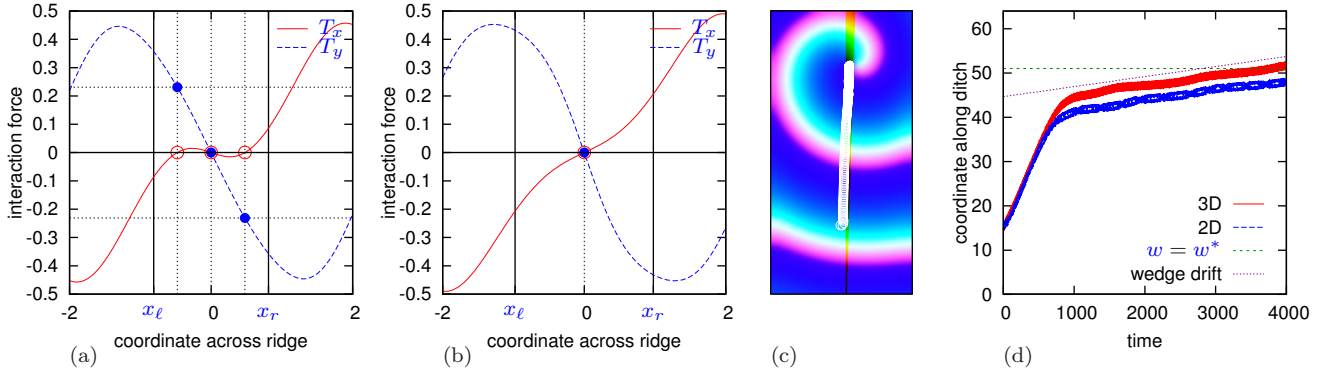


FIG. 3. Results of asymptotic theory of interaction with a ridge/ditch, and comparison with simulations, for FitzHugh-Nagumo system (2). (a,b) Specific interaction force $T(d)$: (a) for $w = 1.621 < w^*$; (b) for $w = 1.953 > w^*$. (c) Spiral wave snapshot (red color component: u field, green color component: v field, blue color component: H field), with the previous tip trajectory (white line), drifting along a cuneiform ditch, of width 0.24 at the lower end and 2.16 at the upper end, box size 32×64 , and $H_o/H_i = 1.2$. (d) Coordinate of the spiral tip along the ditch as a function of time. The horizontal dashed line shows location of the ditch width $w = w^*$ corresponding to the point of the pitchfork bifurcation of $T(d; w)$. The slope of the dotted line represents the slow drift speed due to the sides of the ditch being non-parallel.

the associated correction, let the wedge angle be $\psi \ll 1$. Then the wedge-induced component of the drift speed at the bifurcation point is $2\epsilon S_x(w^*) \sin(\psi/2) \approx \epsilon S_x(w^*) \psi$. For the simulation shown in fig. 3(c,d), we have $\psi \approx 0.03$, and $S_x(w^*) \approx 0.4142$, hence the drift speed $\epsilon \psi S_x(w^*) \approx 0.002266$. This drift speed is represented by the dotted line in fig. 3 and cor-

responds well with the simulations. Finally, let us consider the thickness perturbation of the form

$$H(x, y) = H_0 \left(1 + \epsilon \Theta \left(R_d^2 - (x - x_d)^2 - (y - y_d)^2 \right) \right)$$

i.e. thickening (for $\epsilon > 0$) or thinning (for $\epsilon < 0$) in a disk-

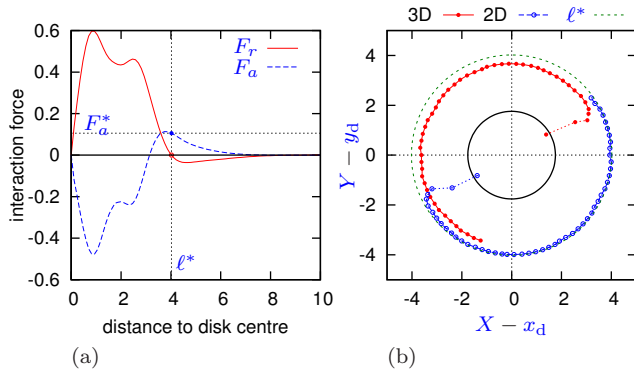


FIG. 4. Interaction of a spiral with a disk-shape bulge in Oregonator model. (a) Components of the interaction force calculated according to (11),(12),(19),(20), for $R_d = 225/1280 \approx 1.756$. (b) Tip trajectories in simulations of duration corresponding to half of predicted orbiting period (lines as indicated by the legend), together with initial transients (thin dotted lines). The green dashed circle: the theoretically predicted stationary orbit of the spiral centre drift. The black solid circle: the boundary of the bulge.

shaped area. Then we have

$$\boldsymbol{\alpha} = \frac{e^{i\vartheta_0} e^{-i\theta} \mathbf{D}}{\pi r \ell \sqrt{1 - \kappa^2}} \left[(\ell \kappa^2 + r \kappa) \mathbf{U}_r - \frac{i \ell (1 - \kappa^2)}{r} \mathbf{U}_\theta \right] \quad (19)$$

for $\vec{r} \in (|R_d - \ell|, R_d + \ell)$, and $\boldsymbol{\alpha} = 0$ otherwise. Here $\ell e^{i\vartheta_0} = (x_d - X) + i(y_d - Y)$ represents the vector from the current spiral centre to the feature centre, and $\kappa = (R_d^2 - \ell^2 - r^2) / ((2r\ell))$. Hence the interaction force is

$$F_x + iF_y = e^{i\vartheta_0} (F_r(\ell) + iF_a(\ell)). \quad (20)$$

The radial $F_r(\ell)$ and the azimuthal $F_a(\ell)$ components calculated for the Oregonator model (3) for an arbitrarily chosen disk radius R_d are shown in Fig. 4(a). We see there is a root of $F_r(\ell)$ at $\ell = \ell^* \approx 4.023$ and the corresponding value of $F_a^* = F_a(\ell^*) \approx 0.1055$ which predicts long-term behaviour of a spiral starting from an appropriate initial condition as “meander” or “orbital movement” along a circle of radius ℓ^* and linear speed ϵF_a^* , that is with the orbit period of $2\pi\ell^*/(\epsilon F_a^*) \approx 1314$. Fig. 4(b) compares these predictions with results of 2D and 3D numerical simulations at $\epsilon = \log(1.2)$. This example is similar to the case considered phenomenologically (simulations and experiment) in [6] and is analogous to “orbital motion” described in [11] for localized parametric heterogeneities.

To summarise, movement of transmural scroll waves through thin layers of excitable media of varying thickness can be approximately described by thickness-averaged two-dimensional equations, and a corresponding 2D perturbation theory can be successfully applied within its limits. This theory shows the propensity of scrolls to interact with sharp features of the layer geometry, which is distinct from and not reducible to previously known geometric effects such as filament tension or curvature-induced drift, and is completely independent from other factors that may cause drift such as

parametric inhomogeneities. Interaction with sharp features can manifest nontrivial attractor structures, depending on the geometric parameters. These predictions should be immediately testable in experiments with the Belousov-Zhabotinsky reaction and may have important implications for understanding of evolution of re-entrant waves excitation in the heart, particularly in atria which have abundance of geometric features.

Acknowledgments H.D. is supported by FWO-Flanders (Belgium). Development of DXSpiral and BeatBox was supported by EPSRC grants EP/D074789/1 and EP/I029664/1 (UK).

-
- [1] A. M. Zhabotinsky and A. N. Zaikin, in *Oscillatory processes in biological and chemical systems*, edited by E. E. Selkov, A. A. Zhabotinsky, and S. E. Shnol (Nauka, Pushchino, 1971) p. 279; M. A. Allesie, F. I. M. Bonke, and F. J. G. Schopman, *Circ. Res.* **33**, 54 (1973); F. Alcantara and M. Monk, *J. Gen. Microbiol.* **85**, 321 (1974); N. A. Gorelova and J. Bures, *J. Neurobiol.* **14**, 353 (1983); B. F. Madore and W. L. Freedman, *Am. Sci.* **75**, 252 (1987); S. Jakubith, H. H. Rotermund, W. Engel, A. von Oertzen, and G. Ertl, *Phys. Rev. Lett.* **65**, 3013 (1990); J. Lechleiter, S. Girard, E. Peralta, and D. Clapham, *Science* **252** (1991); T. Frisch, S. Rica, P. Coullet, and J. M. Gilli, *Phys. Rev. Lett.* **72**, 1471 (1994); M. C. Cross and P. C. Hohenberg, *Rev. Mod. Phys.* **65**, 851 (1993).
 - [2] F. H. Fenton, E. M. Cherry, and L. Glass, *Scholarpedia* **3**, 1665 (2008).
 - [3] V. N. Biktashev, A. V. Holden, and H. Zhang, *Phil. Trans. Roy. Soc. Lond. ser. A* **347**, 611 (1994).
 - [4] H. Dierckx, E. Brisard, H. Vershelde, and A. V. Panfilov, *Phys. Rev. E* **88**, 012908 (2013).
 - [5] T. J. Wu, M. Yashima, F. Xie, C. A. Athill, Y. H. Kim, M. C. Fishbein, Z. Qu, A. Garfinkel, J. N. Weiss, H. S. Karagueuzian, and P. S. Chen, *Circulation Research* **83**, 448 (1998).
 - [6] M. Yamazaki, S. Mironov, C. Taravant, J. Brec, L. M. Vaquero, K. Bandaru, U. M. R. Avula, H. Honjo, I. Kodama, O. Berenfeld, and J. Kalifa, *Cardiovascular Research* **94**, 48 (2012).
 - [7] See EPAPS Document No. [number will be inserted by publisher] for details of asymptotic and numerical procedures. For more information on EPAPS, see <http://www.aip.org/pubservs/epaps.html>.
 - [8] I. V. Biktasheva, D. Barkley, V. N. Biktashev, and A. J. Foulkes, *Phys. Rev. E* **81**, 066202 (2010).
 - [9] I. V. Biktasheva, D. Barkley, V. N. Biktashev, G. V. Bordyugov, and A. J. Foulkes, *Phys. Rev. E* **79**, 056702 (2009), <http://www.csc.liv.ac.uk/~ivb/software/DXSpiral.html>.
 - [10] R. McFarlane and I. V. Biktasheva, in *BCS International Academic Conference “Visions of Computer Science”* (Imperial College London, 2008) <http://empslocal.ex.ac.uk/people/staff/vnb262/software/BeatBox/>.
 - [11] V. N. Biktashev, D. Barkley, and I. V. Biktasheva, *Phys. Rev. Lett.* **104**, 058302 (2010).

Supplementary material: Drift of scroll waves in thin layers caused by thickness features

I.V. Biktasheva, H. Dierckx, V.N. Biktashev

Thin layer asymptotics

When the thickness of the excitable medium layer is much smaller than the diffusion length $\sqrt{|\mathbf{D}|/\max(|\partial\mathbf{f}/\partial\mathbf{v}|)}$, then we can expect the concentration field \mathbf{v} to be nearly constant across the thickness of the layer, thus being effectively a two-dimensional field. To exclude the effects of the curvature we assume the layer to be flat on macroscopic scale. The formal setup is as follows:

$$\begin{aligned} \partial_t \mathbf{v} &= \mathbf{D} \nabla^2 \mathbf{v} + \mathbf{f}(\mathbf{v}), & (x, y) &\in \mathbb{R}^2, & z &\in (z_{\min}(x, y; \mu), z_{\max}(x, y; \mu)), \\ z_{\min}(x, y; \mu) &= 0, & z_{\max}(x, y; \mu) &= H(x, y; \mu) = \mu \tilde{H}(x, y), & \mu &\ll 1, \\ \vec{n}(z_{\min}) \cdot \mathbf{D} \nabla \mathbf{v}(x, y, z_{\min}) &= 0, \\ \vec{n}(z_{\max}) \cdot \mathbf{D} \nabla \mathbf{v}(x, y, z_{\max}) &= 0, \end{aligned}$$

where $\vec{n}(\cdot)$ is the normal vector at the corresponding surface. The shape of the layer is asymmetric and it may seem that variations of thickness may introduce small curvature effects; however it is easy to see that the above formulation is exactly equivalent to a symmetric one,

$$z_{\min}(x, y; \mu) = -\mu \tilde{H}(x, y), \quad z_{\max}(x, y; \mu) = \mu \tilde{H}(x, y).$$

The boundary conditions at $z = z_{\min}$, $z = z_{\max}$ mean that the isosurfaces for the \mathbf{v} concentrations need to intersect the domain boundary perpendicularly. To accommodate this property in our asymptotic solution, we change from the original Cartesian coordinates $\vec{r} = (x^j) = (x, y, z)$ to new curvilinear coordinates $(\rho^j) = (\xi, \eta, \zeta)$, $j = 1, 2, 3$, in the following way:

- Coordinate ζ is “transmural”, that is

$$z(\xi, \eta, 0) = z_{\min}(x(\xi, \eta, 0), y(\xi, \eta, 0)), \quad z(\xi, \eta, 1) = z_{\max}(x(\xi, \eta, 1), y(\xi, \eta, 1)). \quad (21)$$

- The other two “intramural” coordinates (ξ, η) are chosen locally orthogonal to ζ , i.e.

$$\frac{\partial \vec{r}}{\partial \xi} \cdot \frac{\partial \vec{r}}{\partial \zeta} = \frac{\partial \vec{r}}{\partial \eta} \cdot \frac{\partial \vec{r}}{\partial \zeta} = 0. \quad (22)$$

- The intramural coordinates match the horizontal Cartesian coordinates in the sense that

$$x(\xi, \eta, 0) = \xi, \quad y(\xi, \eta, 0) = \eta. \quad (23)$$

Thus the choice of the curvilinear coordinates is fully determined by the choice of function $\zeta(\vec{r})$. A convenient choice is “heat coordinates”, when $\zeta(\vec{r}) = T(\vec{r}; \mu)$ which is a solution of the boundary-value problem

$$\begin{aligned} \nabla^2 T(x, y, z) &= 0, & z &\in (0, \mu \tilde{H}(x, y)); \\ T(x, y, 0) &= 0, \\ T(x, y, \mu \tilde{H}(x, y)) &= 1, \end{aligned} \quad (24)$$

i.e. is identified with an established temperature distribution when a unit temperature drop is imposed across the layer. Then the lines $\xi = \text{const}$, $\eta = \text{const}$ can be interpreted as the lines of heat flux, and in the new coordinates, the boundary conditions become simply condition of zero derivative in ζ , as the vectors \vec{n} are tangent to these flux lines. The two leading terms of the asymptotic of the solution of (24) are

$$T = \frac{z}{\mu \tilde{H}} + \frac{\mu^2 \tilde{H}^2}{6} \left(1 - \frac{z^2}{\mu^2 \tilde{H}^2}\right) \frac{z}{\mu \tilde{H}} \left((\nabla L)^2 - \nabla^2 L\right) + \mathcal{O}(\mu^4); \quad (z \in [0, \mu \tilde{H}])$$

where

$$\tilde{H} = \tilde{H}(x, y), \quad L = L(x, y) = \ln \tilde{H}(x, y).$$

The above derivation was done in the assumption of smoothness of the thickness profile $\tilde{H}(x, y)$. Hence the applications considered in the main paper will be formally covered by this approximation and the 2D spiral perturbation theory, if the ‘‘sharp features’’ considered there are smooth on the scale of \tilde{H} but sharper than the typical scale of the effective response functions’ support. Deviation from this condition in actual 3D simulations may account for some of the discrepancies between the 3D and 2D simulations.

Response functions quadratures

Straight step

The function (13) has a singularity at $r = |d|$, so the resulting integral by r cannot be adequately evaluated by the usual trapezoidal rule. So we proceed instead in the following way. Let the radii grid be $r \in \{j\Delta\rho \mid j = 0, 1, 2, \dots\}$, and $|d| = k\Delta\rho$ for some $k \in \mathbb{Z}_+$. Then we can write, for a regular function $f(r)$ and a $\sigma > -1$,

$$\int_{|d|}^{\infty} f(r)(r^2 - d^2)^\sigma dr = \int_{|d|}^{\infty} F(r)(r - d)^\sigma dr = \sum_{j=k}^{\infty} \int_{j\Delta\rho}^{(j+1)\Delta\rho} F(r)(r - d)^\sigma dr \approx \sum_{j=k}^{\infty} C_j f_j \Delta\rho,$$

where $F(r) = f(r)(r + d)^\sigma$, $f_j = f(j\Delta\rho)$, and linear interpolation of $F(r)$ within each subinterval gives

$$C_j = \begin{cases} \frac{\Delta\rho^{2\sigma}}{2(\sigma+1)} (2k)^\sigma, & j = k, \\ \frac{\Delta\rho^{2\sigma}}{2(\sigma+1)} [(j - k + 1)^{\sigma+1} - (j - k - 1)^{\sigma+1}] (j + k)^\sigma, & j > k. \end{cases}$$

For $\sigma = -1/2$,

$$C_j = \begin{cases} 0, & j < k, \\ \frac{1}{\Delta\rho\sqrt{2k}}, & j = k, \\ \frac{1}{\Delta\rho\sqrt{j+k}} [\sqrt{j-k+1} - \sqrt{j-k-1}], & j > k. \end{cases} \quad (25)$$

In other words, we can use the usual trapezoidal formula, but should multiply $f_j = f(j\Delta\rho)$ by coefficients C_j given above instead of $(r^2 - d^2)^{-1/2} = (r^2 - d^2)^\sigma = (j^2 - k^2)^\sigma \Delta\rho^{2\sigma} = (j^2 - k^2)^{-1/2} \Delta\rho^{-1}$.

Circular step

Similarly, the quadrature for interaction with a disk involves α described by (19), and so is also singular, as it contains denominator $\sqrt{1 - \kappa^2}$ which becomes zero at both ends of the integration interval:

$$\sqrt{1 - \kappa^2} = \frac{1}{2r\ell} [(r - r_{\min})(r_{\max} - r)(r + r_{\min})(r + r_{\max})]^{1/2}$$

where $r_{\min} = |R_d - \ell|$, $r_{\max} = |R_d + \ell|$. Doing as before, we get

$$\int_{r_{\min}}^{r_{\max}} \frac{F(r)}{\sqrt{(r - r_{\min})(r_{\max} - r)}} dr = \sum_{j=0}^N C_j F(r_j) \Delta\rho,$$

where

$$\begin{aligned}
C_0 &= \frac{1}{\Delta\rho^2} [(A_0 - A_1)(r_1 - r_{\text{mid}}) + R_0 - R_1], \\
C_j &= \frac{1}{\Delta\rho^2} [(A_j - A_{j+1})(r_{j+1} - r_{\text{mid}}) + (A_j - A_{j-1})(r_{j-1} - r_{\text{mid}}) + 2R_j - R_{j+1} - R_{j-1}], \quad j = 1, \dots, N-1, \\
C_N &= \frac{1}{\Delta\rho^2} [(A_N - A_{N-1})(r_{N-1} - r_{\text{mid}}) - R_{N-1} + R_N], \\
r_{\text{mid}} &= \frac{1}{2}(r_{\text{min}} + r_{\text{max}}), \\
\Delta\rho &= (r_{\text{max}} - r_{\text{min}})/N, \\
\vec{r}_j &= r_{\text{min}} + j\Delta\rho, \quad j = 0, \dots, N, \\
R_j &= \sqrt{(r_{\text{max}} - r_j)(r_j - r_{\text{min}})}, \\
A_j &= \arcsin\left(\frac{2(r_j - r_{\text{mid}})}{r_{\text{max}} - r_{\text{min}}}\right).
\end{aligned}$$

Discretization

Two-dimensional simulations

We use explicit Euler timestepping with time step Δt and central differencing for the diffusion term in (5), with the following discretization scheme

$$\left[\frac{1}{\tilde{H}} \nabla \cdot (\tilde{H} \nabla \mathbf{u}) \right]_{i,j} = \frac{1}{2\Delta x^2} \frac{1}{\tilde{H}_{i,j}} \sum_{(i',j') \in I} (\tilde{H}_{i+i',j+j'} + \tilde{H}_{i,j}) (\mathbf{u}_{i+i',j+j'} - \mathbf{u}_{i,j})$$

where (i, j) are 2D indices of the regular space grid of the size $N_x \times N_y$ with step Δx and $I = \{(-1, 0), (1, 0), (0, -1), (0, 1)\}$. We employ standard non-flux boundary conditions. The discretization parameters used for different results are described in Table I.

Figure	Δt	Δx	N_x	N_y
2(a,c)	6.4×10^{-4}	8×10^{-2}	400	400
2(d,f)	0.25	1.5×10^{-3}	200	200
3(c,d)	6.4×10^{-4}	8×10^{-2}	400	800
4(b)	0.25	1.5×10^{-3}	200	200

TABLE I. Discretization parameters in 2D simulations

Three-dimensional simulations

The discretization in 3D is a natural extension of the 2D scheme, except instead of a fancy diffusion operator of (5) we now have the plain diffusion of (1). The complication now comes from the more complicated geometry of the domain, which requires special attention to the boundary conditions. We have employed the following discretization:

$$[\nabla^2 \mathbf{v}]_{i,j,k} = \frac{1}{\Delta x^2} \sum_{(i',j',k') \in I} \chi_{i+i',j+j',k+k'} (\mathbf{v}_{i+i',j+j',k+k'} - \mathbf{v}_{i,j,k})$$

where $\chi_{i,j,k} = 1$ if the grid point (i, j, k) is within the domain and 0 otherwise, and the neighbourhood template is $I = \{(-1, 0, 0), (1, 0, 0), (0, -1, 0), (0, 1, 0), (0, 0, -1), (0, 0, 1)\}$. The space grid is regular with step Δx , rectangular $N_x \times N_y$ in the horizontal direction, and with $k \in \{1, \dots, N_z(i, j)\}$ where $N_z(i, j)$ represents the thickness profile. In all our examples, $N_z(i, j)$ takes only two values, denoted as $N_{z,1}$ and $N_{z,2}$. The discretization parameters used for different results are described in Table II.

Figure	Δt	Δx	N_x	N_y	$N_{z,1}/N_{z,2}$
2(c)	6.4×10^{-4}	8×10^{-2}	400	400	1/2, 2/3, 2/4, 3/4, 3/5, 4/5, 4/6, 6/7, 9/10, 14/15, 18/20, 19/20, 38/40, 40/80, 76/80
2(f)	0.25	1.5×10^{-3}	200	200	1/2, 2/4, 3/5, 4/6, 9/10, 18/20, 38/40, 76/80, 2/3, 3/4, 4/5, 6/7, 14/15, 19/20, 40/80
3(d)	6.4×10^{-4}	8×10^{-2}	400	800	5/6
4(b)	0.25	1.5×10^{-3}	200	200	5/6

TABLE II. Discretization parameters in 3D simulations

Response function computations

For `DXSpiral` computations of the FitzHugh-Nagumo model, we use disk radius $\rho_{\max} = 25$, number of radial intervals $N_\rho = 1280$ and number of azimuthal intervals $N_\theta = 64$. For the Oregonator model, we have correspondingly $\rho_{\max} = 15$, $N_\rho = 128$ and $N_\theta = 64$.
